Available online at www.sciencedirect.com
ScienceDirect
International Journal of Heat and Mass Transfer 50 (2007) 3966–3976
International Journal of HEAT and MASS TRANSFER
www.elsevier.com/locate/ijhmt

Bubble jet flow formation during boiling of subcooled water on fine wires

J.F. Lu, X.F. Peng *

Laboratory of Phase-change and Interfacial Transport Phenomena, Department of Thermal Engineering, Tsinghua University, Beijing 100084, China

Received 8 October 2005; received in revised form 4 May 2006
Available online 12 April 2007

Abstract

Both visual technology and numerical simulation were employed to investigate bubble jet flow formation during boiling of subcooled water on ultrathin platinum wires. Experimental observations and measurements indicated that bubble jet flow formation could be typically divided into three stages: waiting, burst and stably developing stage. A transient numerical model was proposed to simulate the formation process accounting for the thermocapillary force existing at the bubble interface. The dynamical temperature variation in the liquid region, including the regions of the mushroom head and root stem, were numerically analyzed, showing a very good agreement with the experimental observations. The simulation very well explored the physical nature of the dynamical evolution of bubble jet flows and explained the experimental phenomena.

Keywords: Bubble-top jet flow; Thermocapillary force; Visual observation; Numerical simulation

1. Introduction

Understanding boiling is still one of the most challenging problems for its complexity and diversity [1,2]. Since the urgent demand for practical applications in developing high technologies associated with liquid–vapor phase change, researchers paid great attention to explore and understand the boiling phenomena, such as nucleation, nucleate, transition and film boiling, bubble dynamics, and their physical nature. In the last two decades, boiling was comprehensively investigated for some special cases, or those under microscale, microgravity conditions [3,4], at high subcooling and/or high superheat conditions [5,6], and some other special conditions with electromagnetic effects [7]. Microlayer evaporation [8–10] and jet flows [11,12] were emphasized in recognizing new phenomena and understanding boiling mechanisms from new aspects. So far, these fundamental investigations are still far from truly understanding the boiling phenomena, particularly providing an effective methodology to predict the boiling heat transfer and understand the fundamental mechanism.

Bubble dynamics and associated flows were considered as important complements to nucleate boiling heat transfer. Forster et al. [13,14] investigated the effect of flow caused by vapor bubbles on the boiling heat transfer, and they proposed a boiling heat transfer mechanism model in which a bubble was treated like a pump driving the hot liquid into the bulk liquid. Shekriladze et al. [15,16] observed bubble-top jet flows ejecting from the bubble top into the bulk liquid, and presumed that the interfacial mass flux due to evaporation and condensation at the interface played an important role in these phenomena. Peng with different co-researchers [17–19] experimentally investigated nucleation and bubble-top jet flows on small wires, and found the jet flow played a key role in boiling heat transfer. Apparently, these researchers tried to understand and predict the boiling heat transfer from different aspects concerning with interfacial effects. Available articles have

* Corresponding author. Tel./fax: +86 10 6278 9751.
E-mail address: pxf-dte@mail.tsinghua.edu.cn (X.F. Peng).

0017-9310/$ - see front matter © 2007 Published by Elsevier Ltd.
doi:10.1016/j.ijheatmasstransfer.2007.01.055

Nomenclature

c	thermal capacity (J K^{-1} kg^{-1})
h	heat transfer coefficient (W m^{-2} K^{-1})
h_{fg}	latent heat (J kg^{-1})
$\overline{M}$	molecular weight (kg kmol^{-1})
p	pressure (Pa)
q''	heat flux (W m^{-2})
$\overline{R}$	universal gas constant (J kmol^{-1} K^{-1})
r	radius (m)
T	temperature (K)
t	time (s)
u	velocity (m s^{-1})
V	velocity vector (m s^{-1})

Greek symbols

λ	conductivity (W m^{-1} K^{-1})
σ	interfacial tension (J m^{-2})
$\hat{\sigma}$	accommodation coefficient (–)
ρ	density (kg m^{-3})
μ	viscosity (kg m^{-1} s^{-1})

Subscripts

b	bubble
D	width
H	height
i	interface
sat	saturation
v	vapor
w	wire

provided adequate investigations on the steady jet flow phenomena, while the unsteady jet flow phenomena, like jet flow formation process, should be further studied.

Various simulation models in the open literature were mainly devoted to the steady jet flow phenomena caused by the thermocapillary force. Marek and Straub [20] investigated the thermocapillary convection induced by the temperature gradient along a bubble interface during subcooled pool boiling, and meanwhile they considered the significant effects of non-condensable gas. Christopher et al. [21] conducted a similarity simulation for Marangoni convection around a vapor bubble during nucleation and growth. Wang et al. [22] proposed a numerical model to simulate the steady bubble-top jet flows during subcooled boiling on wires. These investigations showed that the simulation based on the boiling mechanism was useful for understanding the boiling phenomena.

This paper mainly presented experimental measurements and the associated simulation for jet flow formation. A transient numerical model was proposed to simulate the formation process accounting for the thermocapillary force existing at the bubble interface, and the simulation results were compared with experimental observations. The simulation satisfactorily described the experimental phenomena and explored the mechanism of the bubble jet flow formation.

2. Experimental facility

The experimental facility employed in current investigation mainly consisted of three parts, including the test section, power supplier and acquisition system, as illustrated in Fig. 1. The test module was a vessel with a dimension of 250 × 250 × 400 mm (length × width × height) (1), and was made of stainless steel, with two glass windows opened oppositely on its two sides. Two copper electrodes (5) of

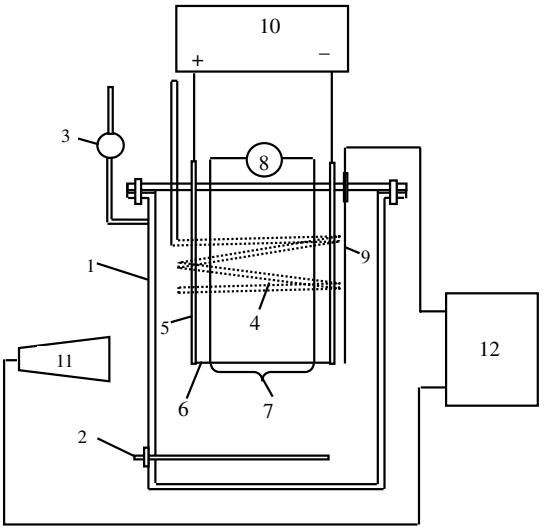

Fig. 1. Schematics of testing block: (1) vessel, (2) pre-heater, (3) pressure gauge, (4) cooler, (5) electrode, (6) wire heater, (7) tested section, (8) voltage gauge, (9) thermocouples, (10) power supply, (11) CCD camera, (12) personal computer.

diameter 5 mm were installed on the cover, and a wire heater (6) was horizontally connected to two electrodes and placed in the vessel. The heated wires made of platinum or tungsten was about 80–100 mm long, and their diameters ranged from 100 to 240 μm. A pre-heater (2) and cooler (4) were included in the test module to control the bulk liquid temperature. A gas valve and pressure gauge (3) were also installed, and the pressure was kept at the atmospheric pressure in the present experiments.

The power supplier (10) was a HP Agilent Model-6031A system, which can provide a maximum voltage of 20 V and maximum power of 1000 W. Direct current was applied to the wire, and a uniform heat flux was generated to heat the liquid. To reduce the boundary effect of electrodes, the

middle region of the wire was selected as the test section (7), and the voltage was measured directly by a voltage gauge (8). The experiments employed pure water as working fluid, which was boiled to reduce the dissolved air before experimental measurements.

The acquisition system included two sub-systems, or image acquisition and data acquisition, and a personal computer (12) was used to collect and store the images and data. The photographic system consisted of a high-speed CCD camera (the Motionscope PCI, Redlake imaging), a high-resolution image acquisition card, and zoom lenses. The CCD camera (11) can reach a high speed up to 2000 frames per second. The present experiments used the rate of 500fps and the resolution of 320×280 pixels.

The data acquisition system was Keithley 2700 multimeter system, and the error of voltage measurement was less than 0.1 μV (0.005 K for temperature measurement). A T-type thermocouples (9) was used to measure the bulk liquid temperature, and its uncertainty was about ±0.2 K. The current and voltage of the tested section were measured to determine the applied heat flux, and the average wire temperature was estimated from the wire resistance by the calibrated correlation. The resistance of the wire was pre-calibrated as an approximately linear function of temperature, so the temperature change of the tested section could be obtained from the measurement of the resistance. An error analysis showed the overall uncertainty of the wire temperature measurement was ±2 K, while the uncertainty of the heat flux was ±2%.

3. Bubble jet flow formation

For subcooled boiling at moderate heat fluxes, bubble jet flows and complex bubble dynamical characteristics were clearly observed by the CCD system at proper light illumination. The bubble dynamics and associated phenomena observed were similar for wires of different diameters or materials.

Bubble jet flows were visually observed forming on the wires and penetrating into the bulk liquid in present experiments. The whole process explored an entire lifetime of a bubble jet flow. A bubble jet flow usually generated when the bubble was very small, and its formation process lasted about 0.020–0.200 s that was much shorter than a bubble departure period. After its formation, a bubble jet flow could continue until the bubble lost its stability due to departure or collision. In the experiments, bubble jet flows were normally above small bubbles whose radiuses ranged from 0.01 mm to 0.30 mm, and the length of jet flows were about 0.5–2.0 mm. In present investigation, the attention would be mainly addressed on the bubble jet formation process, and the bubble radius was usually in the range of about 0.01–0.04 mm during the formation process.

Fig. 2 presents the formation process of a bubble jet flow during subcooled boiling on a tungsten wire having diameter of 200 μm at bulk liquid temperature of 36 °C and heat flux 0.60×10^6 W m^{-2}. At the beginning, a small bubble formed on the wire, and a high temperature region correspondingly appeared near the bubble interface. At 0.040 s, the high temperature region still had no obvious variation. After about 0.050 s, the high temperature region began to develop quickly, and a mushroom-like cloud or a pre bubble jet flow formed around the bubble at 0.060 s. In the next 0.020 s, the cloud quickly evolved and gradually converged to an embryo jet flow. At 0.110 s, the head of the jet flow began to diffuse into the bulk liquid. After that, the mushroom-like cloud would finally evolve and converge to a fully-developed bubble jet flow extending into the bulk liquid. During the formation process, the bubble size had no significant change, and its radius was about 0.035 mm.

Generally, the bubble jet flow formation process can be divided into three stages, as illustrated in Fig. 2, and similar phenomena were observed in various subcooled boiling on different thin wires of diameter 0.1–0.24 mm in present investigation. Before 0.050 s, no clear jet flow image was observed around the bubble, therefore this stage can be

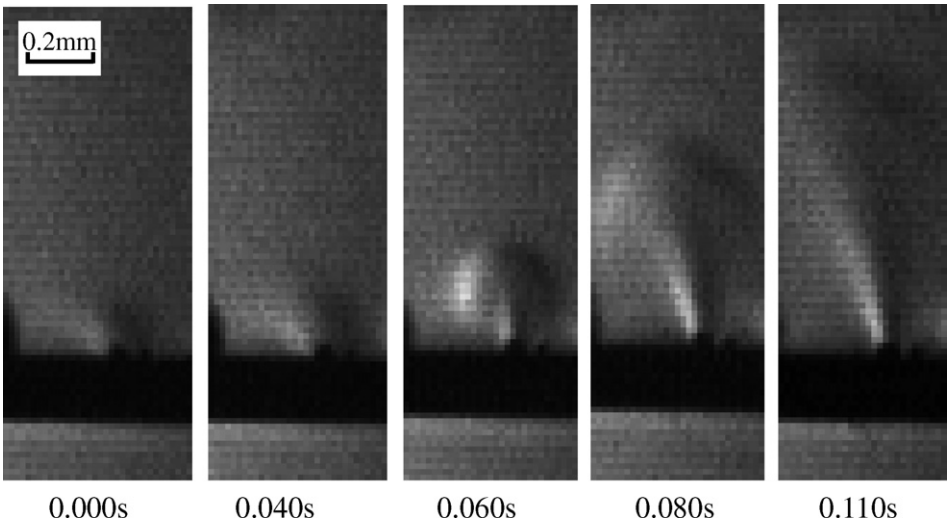

Fig. 2. Bubble jet flow formation ($T_w = 36\,^{\circ}C$, $q''_w = 0.60 \times 10^6$ W m^{-2}).

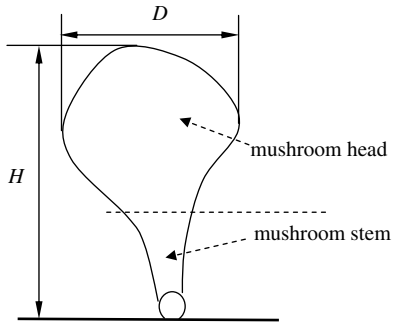

Fig. 3. Structure of a bubble jet.

considered as a waiting stage. From 0.050 s to 0.080 s, the bubble jet flow formed and expanded rapidly, and this was a burst stage. After 0.080 s, the bubble jet flow evolved into a stable jet flow, and it was a stably developing stage. Typically, the mushroom-like cloud during the burst stage can be divided into two main regions: mushroom stem and mushroom head, as shown in Fig. 3. The mushroom stem was a jet flow with strong intensity just above the bubble, and it kept stable during the developing stage. The mushroom head was the front of the jet flow, and it would merge into the bulk liquid to form a fully-developed jet flow.

For a quantitatively investigation, a jet flow can be described with its geometrical parameters of height, H, and width, D, as illustrated in Fig. 3. The detail information of the dynamical behavior in Fig. 2 is illustrated in Fig. 4, where $u_H = \mathrm{d}H/\mathrm{d}t$, $u_D = \mathrm{d}D/\mathrm{d}t$, and this expansion velocity was directly dependent upon the Marangoni flow drove by the bubble. In the waiting period of 0.000–0.050 s, the jet flow front or parameter H varied only from 0.17 mm to 0.26 mm, and the expansion velocity along the height was lower than 4 mm/s. During 0.050–0.080 s, the jet flow burst and the height rapidly changed from 0.26 mm to 0.71 mm. It approached its maximum vertical expansion velocity of 22 mm/s at 0.7 mm away from the wire. After 0.080 s, the jet flow front seemed to reach an invariable velocity about 8 mm/s, and the front would submerge into the bulk liquid as the time going on. In Fig. 4, the jet flow expansion velocity had a jump at about 0.050 s, and this can be identified as the transition time from the waiting stage to burst stage.

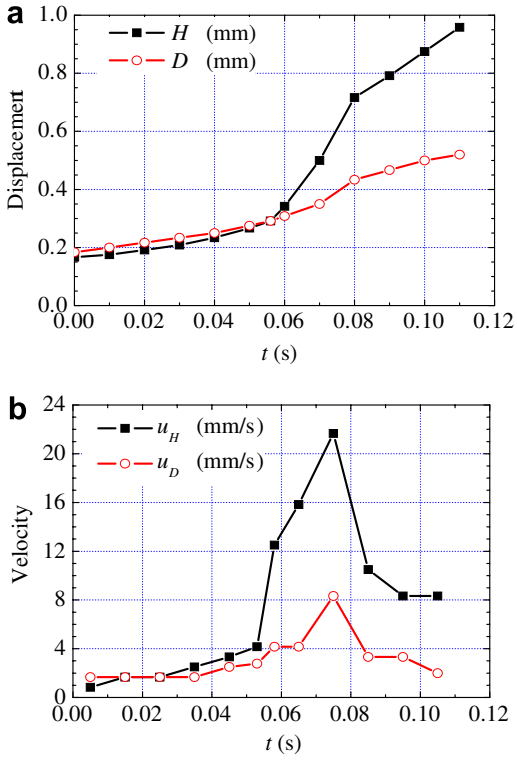

Fig. 4. Behavior of a jet flow formation: (a) jet flow geometry, (b) expansion velocity.

During the whole dynamical process, the width of a jet flow expanded more slowly than its height, and that meant the upward flow dominated the jet flow. In addition, since the basic jet flow configuration was similar during the short burst stage, the velocity along the height and width reached the maximum values almost at the same time, as illustrated in Fig. 4.

During bubble jet flow formation, the radius of the bubble grew only a little. Consequently, the interfacial tension should have critical influence on bubble dynamics comparing with the buoyancy due to the gravitation force. Marek and Straub [20] investigated the thermocapillary convection existing in subcooled nucleate boiling. Christopher et al. [21] considered Marangoni convection around a vapor bubble during nucleation and growth. Wang et al. [22] indicated that the velocity of natural convection near a small bubble had a magnitude of 0.002 m/s, and the Marangoni flow due to the surface tension gradient induced much stronger liquid flow than the natural convection with velocity magnitude of 0.020–0.040 m/s. From these investigations, the thermocapillary force due to interfacial temperature gradient should certainly be considered to play a significant role in the bubble jet flow generation, especially under microgravity condition or situations in which the gravitation is not significant. With heat transport between the bubble and surrounding liquid, the condensation and evaporation along the interface would be important to the temperature distribution along the bubble, therefore would greatly affected the jet flow behavior.

4. Simulation model

4.1. Fundamental consideration

As noted in many previous investigations, thermocapillary flow driven by interfacial tension gradient is expected to play a principal role in bubble-top jet flow phenomena. During bubble jet flow formation in the experiments, the diameter of a bubble is usually about 0.02–0.08 mm, and the jet velocity is about 10–50 mm/s. From the experiment results in Fig. 2, $r_b = 0.035$ mm, $u = 20$ mm/s, $v \approx 5.0 \times 10^{-7}$ m^2 s^{-1}, and $Re = 0.7$. So the laminar model is adopted

in this simulation, and the governing equations in the fluid zone (water) are given as:

$$\nabla \cdot (\rho V) = 0 \tag{1a}$$

$$V \cdot \nabla V = v \cdot \nabla^2 V - \frac{\nabla p}{\rho} - g \cdot j \tag{1b}$$

$$V \cdot \nabla (c \cdot T) = \frac{1}{\rho} \lambda \nabla^2 T \tag{1c}$$

where j denotes the unit vector in the vertical direction. The properties of the working liquid and associated constant are specified as $c = 4182\ \mathrm{J\ kg^{-1}\ K^{-1}}$, $\lambda = 0.6\ \mathrm{W\ m^{-1}\ K^{-1}}$, $g = 9.8\ \mathrm{m\ s^{-2}}$. The piecewise-linear model is employed to describe the viscosity and density, as illustrated in Fig. 5 [23], and the natural convection due to density difference can then also be computed. Eq. (1) is solved using a finite volume method, and the second order upwind differentiating is used to approach a converged solution. In present simulations, the numerical results converge with the time, and the residual errors of velocity and energy are set smaller than 10^{-5}.

Inside the bubble, the vapor temperature is equal to the saturation temperature corresponding to the local pressure. For a growing bubble, the local pressure inside the bubble is obtained from Rayleigh equation [24,25]

$$P_v - P_0 = \frac{2\sigma}{r_b} + \rho_l \left[R \frac{d^2 r_b}{dt^2} + \frac{3}{2} \left(\frac{dr_b}{dt} \right)^2 \right] \tag{2a}$$

where P_0 is the liquid pressure outside the bubble. And the temperature inside the bubble is solved from Clausius–Clapeyron equation [1]:

$$T_v = T(P_v) = T_{sat}(P_0) + \frac{2\sigma T_{ssat}}{h_{fg} \rho_v r_b} + \frac{T_{ssat} \rho_l}{h_{fg} \rho_v} \left[r_b \frac{d^2 r_b}{dt^2} + \frac{3}{2} \left(\frac{dr_b}{dt} \right)^2 \right] \tag{2b}$$

For the bubble during the jet formation process in Fig. 2, $r_b = 0.035$ mm, $dr_b/dt < 10^{-3}\ \mathrm{m\ s^{-1}}$, $d^2 r_b/dt^2 < 10^{-2}\ \mathrm{m\ s^{-2}}$, the temperature correction due to the interfacial tension in Eq. (2) is only about 0.3 °C, so it is reasonable to assume $T_v \approx T_{sat} = 373$ K in the calculation.

The phase-change heat transfer occurring at the interface of the bubble can be expressed as [1]

$$q = h \cdot (T_{li} - T_v) \tag{3a}$$

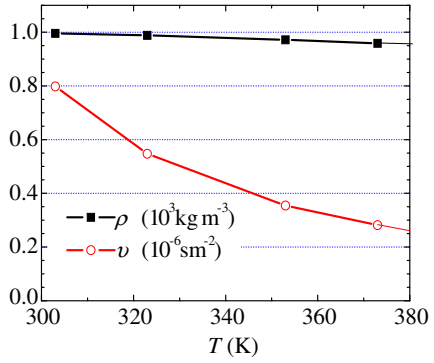

Fig. 5. Fluid viscosity and density [21].

where T_{li} is the liquid temperature adjacent to the interface, and accordingly the heat transfer coefficient is [1]

$$h = \frac{2\hat{\sigma}}{2 - \hat{\sigma}} \frac{h_{fg}^2 \rho_v}{T_v} \left(\frac{\overline{M}}{2\pi \overline{R} T_v} \right)^{1/2} \left[1 - \frac{p_v}{2 h_{fg} \rho_v} \right] \tag{3b}$$

where $\overline{M}$ and $\overline{R}$ are molecular weight and universal gas constant, respectively. The accommodation coefficient $\hat{\sigma}$ is generally assumed to be 0.02–0.04 for water [1], and here the heat transfer coefficient is taken as $h = 2.0 \times 10^5\ \mathrm{W\ m^{-2}\ K^{-1}}$ for $\hat{\sigma} = 0.025$.

4.2. Dynamical model

For convenience and simplification, a dynamical model is proposed to consider different evolution stages separately, or the waiting stage without thermocapillary force, and both the burst and stably developing stage with thermocapillary force.

According to experimental results, during the waiting stage the temperature field and jet flow develop very slowly, and the thermocapillary force has no significant effect on the flow field around bubble. The main result in this stage is the establishment of temperature gradient along the bubble interface. This is caused by the conduction and weak natural convection in the liquid, and the thermocapillary force is ignored in this stage. A steady temperature field is consequently derived for investigating the dynamical behavior of the next two stages, and this is actually preliminary phenomenon for the jet flow formation.

In the burst and stably developing stage, the jet flow is significantly developed, and the thermocapillary force plays a principle role. Correspondingly, the boundary condition for the momentum equation at the bubble interface is modeled using the Marangoni boundary condition as:

$$-\mu \left(\frac{\partial V_s}{\partial n} \right)_X = \frac{\partial \sigma}{\partial T} \left(\frac{\partial T}{\partial s} \right)_X \tag{4}$$

where n and s indicate the normal and tangential direction to the interface, respectively, X, the interface, and $\partial\sigma/\partial T = -1.8 \times 10^{-4}\ \mathrm{N\ m^{-1}\ K^{-1}}$.

In the simulation, the steady temperature and flow field in the waiting stage, obtained by the model without thermocapillary force, is used as initial conditions for the jet formation in burst and stably developing stage, and then the whole jet formation phenomena can be analyzed. In both Figs. 2 and 4, the jet flow scale and expansion velocity began to significantly increase at 0.050 s, and the waiting time was about 0.050 s.

4.3. Calculation domain

In order to demonstrate the jet formation process in detail, the present work will mainly investigate the flow around a single bubble attaching on a heating wire, and the associated geometrical parameters are illustrated in Fig. 2. Since the bubble shape almost kept invariable dur-

ing bubble jet flow formation, a spherical bubble is assumed, and $r_w = 0.200$ mm, $r_b = 0.035$ mm, as shown in Fig. 6. Additionally, there is normally a microlayer between the bubble and wire, and available investigations indicated that the microlayer thickness could be taken as 0.5–2.5 μm [26]. In present calculation, the bubble is settled above the wire with a minimum distance of 2 μm, and the investigations for different situations show that the thickness of microlayer only has little effect on the characteristics of bubble jet formation.

The calculation domain is a horizontal column with diameter 4 mm and length 1 mm, referring to Fig. 6. The system is periodic along x-axis, and only half of the system is calculated for the symmetry at $z = 0$ (or x–y plane). The calculation results show that the system is large enough for analyzing bubble jet flow formation with very little boundary effects. The grid in Fig. 6 includes about 66,000 elements of tetrahedron and hexahedron, which was checked as an appropriate one. In present calculations, the temperature of the wire surface is set to 380 K, while the outer boundary conditions are at a specified bulk liquid temperature 303 K and atmosphere pressure. These are very much close to the experimental situations.

5. Temperature evolution

5.1. General behavior

The dynamic temperature variation around a specified bubble during bubble jet flow formation is illustrated in Fig. 7. During the waiting stage or at $t = 0.000$ s, the thermal boundary layer (here assume $T_{sub} < 30$ K) near the wire has a thickness of 0.3 mm, and a high temperature region, a very thin layer is observed around the bubble. Before 0.010 s, the high temperature region is still within the thermal boundary layer, and the bubble jet flow is not obvious. After 0.010 s, the high temperature region pushes the thermal boundary layer into the cold liquid, and the bubble jet begins to develop. In a short time, the jet flow with high temperature quickly bursts, and both the center and boundary extend rapidly. As the experimental images shown in Fig. 2, both mushroom head and stem extended and penetrated far away within 0.040 s (from 0.040 s to 0.080 s). After 0.060 s, the stem of the jet flow became stable, while the top of the jet flow still continued to extend into the bulk liquid. Comparing with Figs. 2 and 7a, the calculation results in the vertical plane across the wire are in a reasonable agreement with the experimental observations, clearly showing three main stages in the bubble jet flow evolution. In the vertical plane normal to the wire as Fig. 7b, the temperature decreases to the bulk liquid temperature quickly from jet flow region. Fig. 8 illustrates more detail temperature information during the bubble jet formation.

5.2. Temperature evolution on the bubble interface

The temperature on the spherical surface of the bubble is illustrated in Fig. 9. At initial time, the temperature increases along the interface approaching to the wire, and there is a cold spot just on the top of bubble. In present simulations, this steady temperature distribution without thermocapillary force occurs in the waiting stage. During 0.000–0.010 s, the jet flow changes rapidly from waiting stage to bursting stage. After the transition or initial stages, the thermocapillary convection flow quickly makes the temperature in the upper region of the bubble interface uniform, only the temperature at the bubble interface near the wire still changes obviously, and this is quite different from that in the waiting stage.

After 0.010 s, two cold areas appear near the middle region of the bubble interface on the two side surfaces sym-

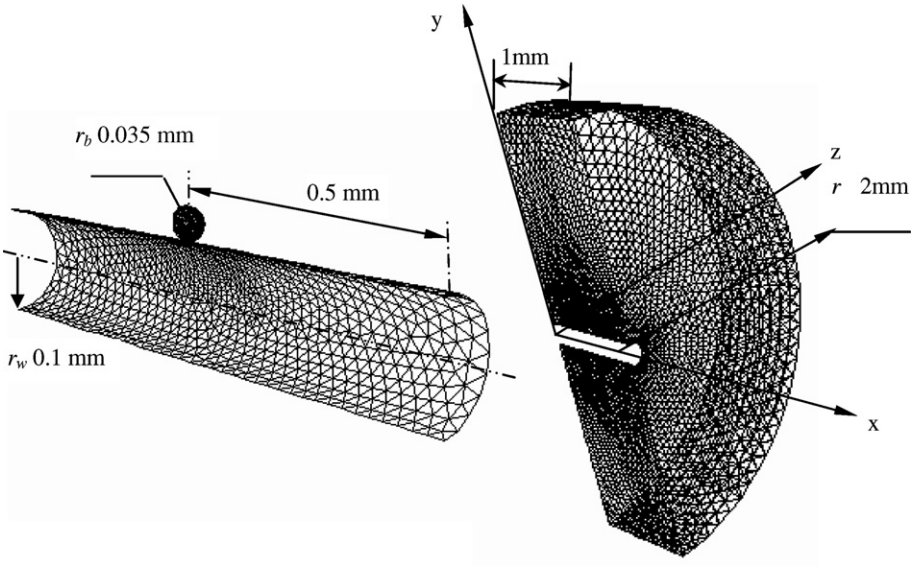

Fig. 6. Model for bubble jet flow formation.

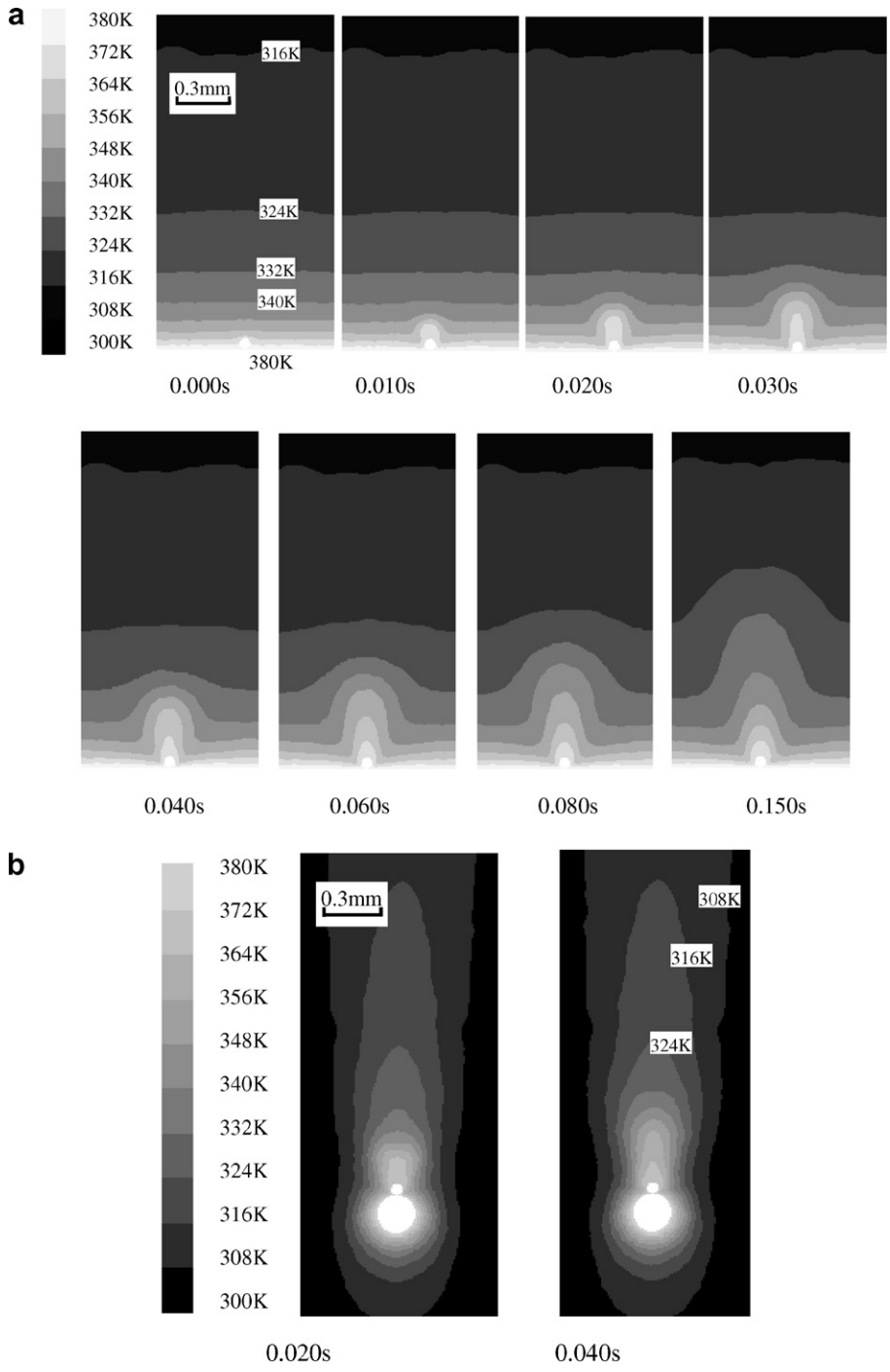

Fig. 7. Temperature evolution during jet flow formation: (a) the vertical plane across wire axis ($z = 0$ mm), (b) the vertical plane normal to the wire ($x = 0.5$ mm).

metrical about the wire axis, respectively, and they expand before 0.030 s. From 0.030 s to 0.060 s, the cold area shrinks, and the temperature in the upper region on the bubble becomes uniform again. After the 0.060 s, and the temperature profile on the bubble interface has very little variation.

From the temperature evolution on the bubble interface, two special phenomena can be identified clearly. The cold region on the bubble interface occurs in the middle region of the bubble during burst and fully developed stages, and another important phenomenon is that a lowest surface temperature in the cold region appears during the burst stage. These phenomena are mainly caused by the coupling effect of the jet flow and temperature field. Because of the spatial limit, the pumping and cooling effect in the bubble interface region exactly above the wire is weaker than that in the two bubble side regions symmetrical about the wire, then two cold patches occur on two side regions at the

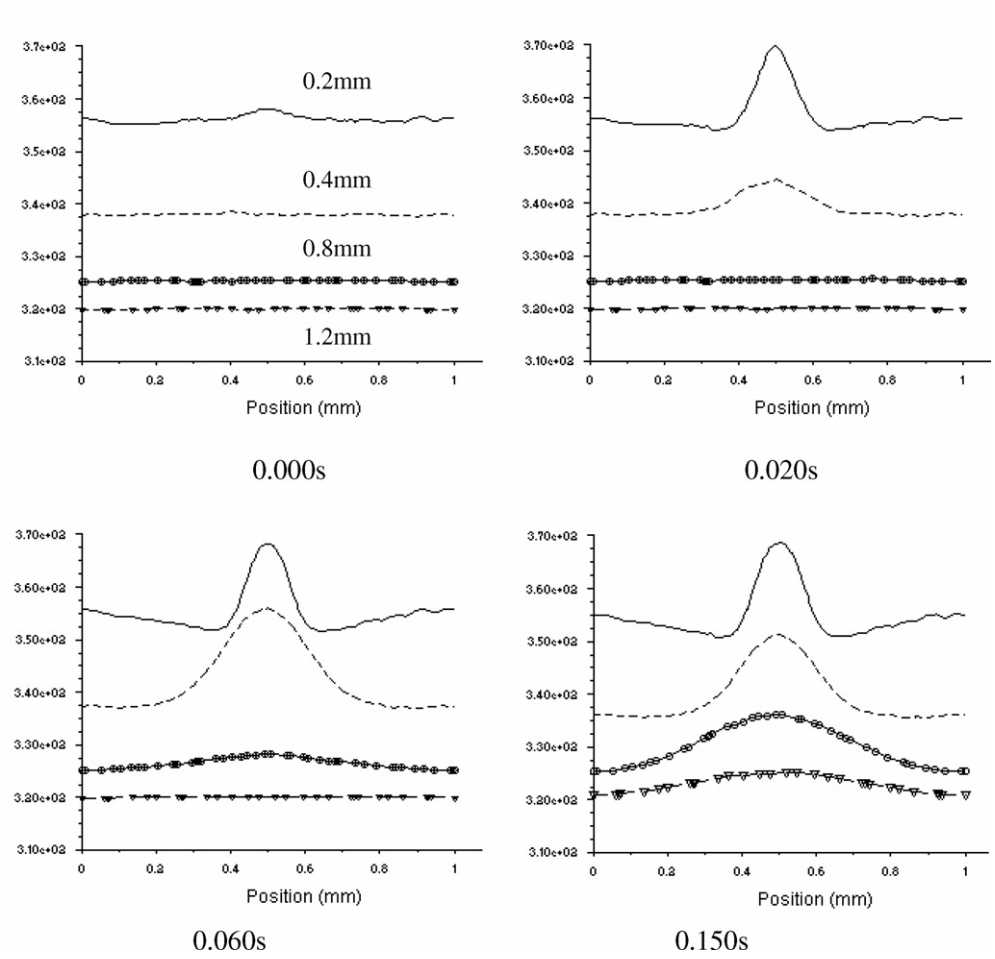

Fig. 8. Temperature field above the wire.

interface. Furthermore, since the velocity of jet flow formation reaches its maximum value during burst stage as illustrated in Fig. 4, the thermal boundary layer near two sides of the bubble will reach a minimum value, and the lowest temperature of the cold region will also be reached.

6. Flow evolution

The dynamical evolution of the flow field is presented in Fig. 10, corresponding to the situation of Fig. 7. At the initial stage or waiting stage, natural convection contributes to the flow as a principle mechanism, and the jet flow around the bubble has little effect on the bulk liquid. After the waiting stage, the interfacial thermocapillary force becomes to drive the liquid, but the jet flow is still within the thermal boundary layer in the first 0.010 s.

During 0.010–0.030 s, two cold areas appear near the middle region on both sides of the bubble surfaces which symmetrically distributes along the wire axis, respectively, referring to Fig. 9, and this would cause special flow field because the interfacial thermocapillary force will drive the liquid from the hot region to cold region. In the vertical plane across the wire axis, the liquid at the bubble top will be driven downwards to the cold region, while the liquid at the bubble bottom is pumped upwards. As a result, the jet flow will disperse above the bubble, and that is just like a mushroom cloud as in Fig. 2.

From 0.030 to 0.060 s, two cold areas shrink, and the temperature in the upper region on the bubble becomes uniform. Apparently, the flow from the bubble top to middle region would decrease quickly, and the mushroom correspondingly evolves and converges to a strong jet flow, as illustrated in Figs. 2 and 10.

After 0.060 s, the structure of interface temperature distribution is almost invariable. As a result, the mushroom stem also keeps its shape. On the other hand, the mushroom head penetrates into the bulk liquid and gradually mixes with the bulk liquid. Finally, a fully-developed jet flow forms. In this stage, the jet flow and its temperature profile evolve stably and can last a long time.

During the bubble jet formation, the temperature gradient at the bubble interface first causes thermocapillary flow near the bubble, and then the flow extends above the bubble. Because of the hot liquid flow from the region near the bubble or wire, the temperature of the liquid above the bubble increases significantly. As a result, both flow field and temperature profile are coupled with each other. Apparently, the bubble jet flow certainly plays an impor-

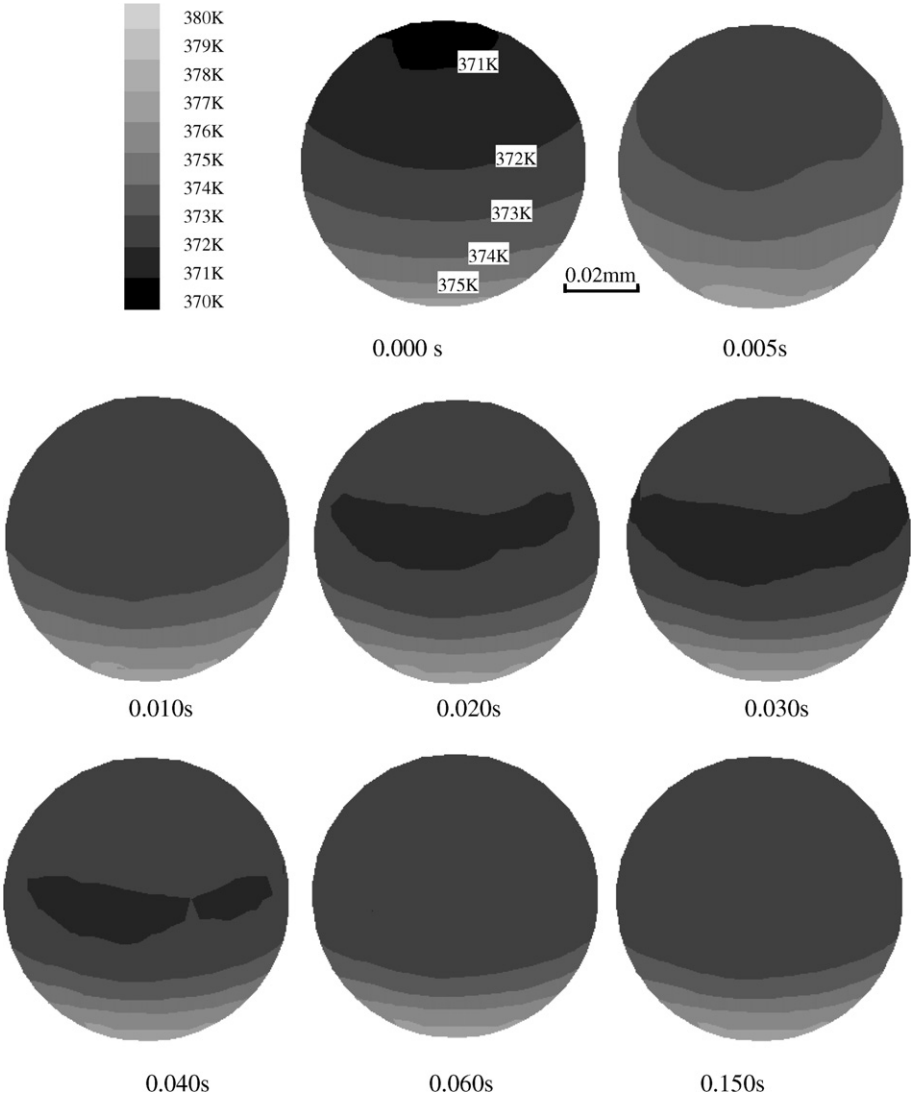

Fig. 9. Temperature evolution on a bubble surface.

tant role in boiling heat transfer due to liquid pumped from the hot region to the cold region.

In the experiments, the jet flow can be considered as a region with high velocity above the bubble. Corresponding to the simulation results in Fig. 10, the jet flow region can also be identified as the region with velocity $u > u_0$ above the bubble. The velocity level u_0 is predicted by the comparison of experimental and simulation results. In order to compare Figs. 2 and 10, we should add the waiting time or 0.050 s to the time in simulation. The jet flow geometry in simulation with its geometrical parameters of height, H, and width, D is illustrated in Fig. 11, where $u_0 = 6$ mm/s and the jet flow region is just the bright region in Fig. 10.

Compared the simulated results in Fig. 11 with experimental results in Fig. 4a, the scale of jet flow in simulation is apparently underestimated just after the waiting stage or during 0.050–0.060 s, because the present model ignores the thermocapillary force in the waiting stage. During the main burst stage and developing stage or after 0.060 s, the dynamical characteristics of jet structure agree well with those of the experiments.

7. Conclusions

In this investigation bubble jet flow formation was experimentally and numerically investigated during subcooled boiling on ultrathin platinum wires. The dynamical evolution of bubble jet flow was visually observed and quantitatively measured. The bubble jet flow can be typically divided into two main regions: mushroom stem and mushroom head. Bubble jet flow formation normally includes three stages, waiting, burst and stably developing stage. By considering the thermocapillary force and heat transfer on the bubble interface, a transient numerical model was proposed to simulate the dynamical formation of a bubble jet flow. The dynamical temperature evolution on the bubble surface and above the bubble was described and discussed theoretically. The simulation explored the physical nature of the bubble jet flow formation and very

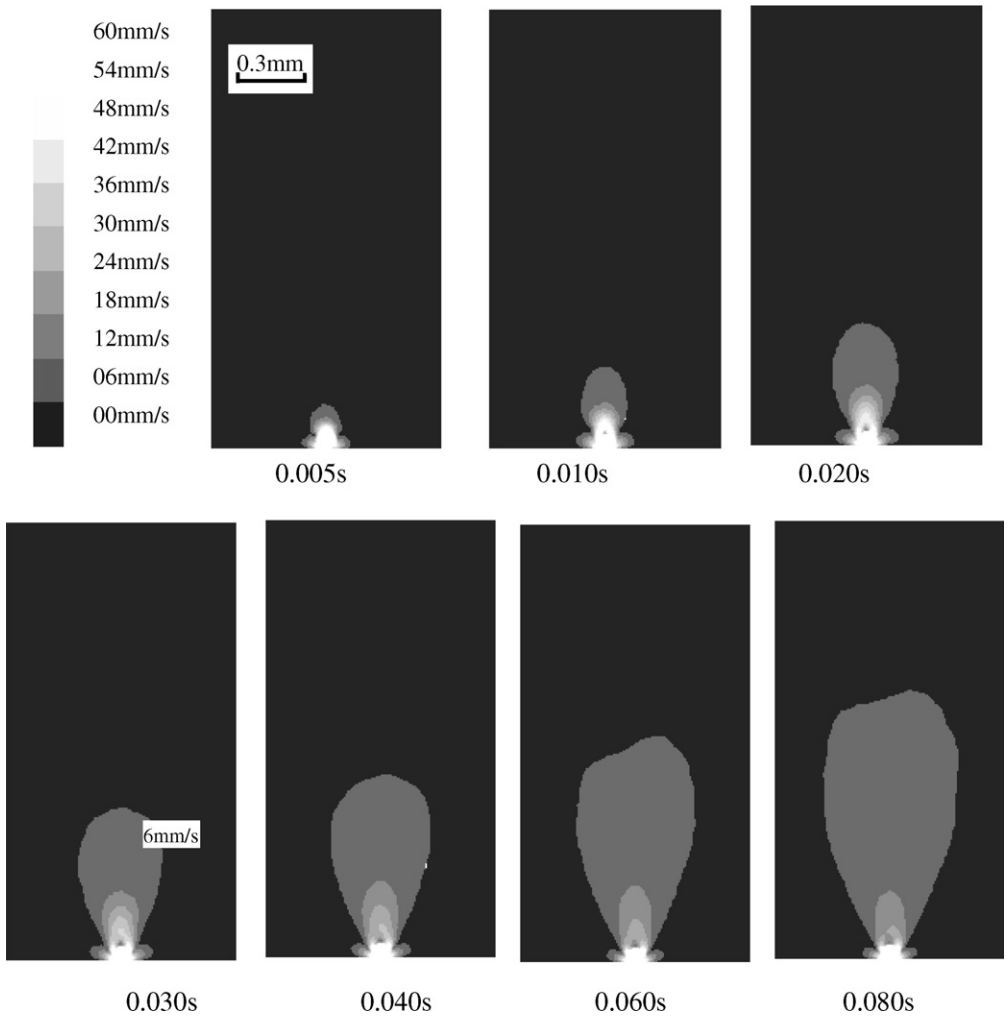

Fig. 10. Flow evolution around a bubble.

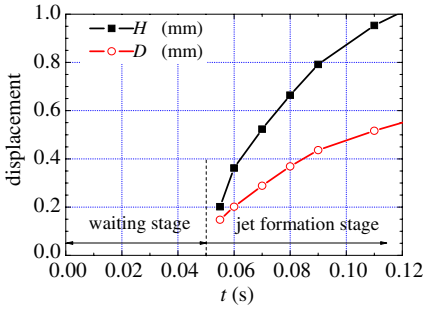

Fig. 11. Jet flow geometry in simulation ($u > 6$ mm/s).

well explained the experimental phenomena, and the jet structure showed a good agreement with the experimental observations.

Acknowledgements

This research is currently supported by the National Natural Science Foundation of China. (Contract No. 90505012) and the Specialized Research Fund for the Doctoral Program of High Education (Contract No. 20040003076).

References

[1] V.P. Carey, Liquid–Vapor Phase-change Phenomena: An Introduction to the Thermophysics of Vaporization and Condensation Processes in Heat Transfer Equipment, Hemisphere Pub. Corp., New York, 1992.
[2] V.K. Dhir, Nucleate and transition boiling heat transfer under pool boiling and external flow conditions, in: Proc. 9th Int. Heat Transfer Conf., Jerusalem, Israel, vol. 1, 1990, pp. 129–155.
[3] X.F. Peng, H.Y. Hu, B.X. Wang, Boiling nucleation during liquid flow in microchannels, Int. J. Heat Mass Transfer 41 (1) (1998) 101–110.
[4] J. Straub, Microscale boiling heat transfer under 0g and 1g conditions, Int. J. Therm. Sci. 39 (2000) 490–497.
[5] L.W. Lin, Microscale thermal bubble formation—thermal physical phenomena and applications, Microscale Thermophys. Eng. 2 (2) (1998) 71–82.
[6] S. Glod, D. Poulikakos, Z. Zhao, G. Yadigaroglu, An investigation of microscale explosive vaporization of water on an ultrathin Pt wire, Int. J. Heat Mass Transfer 45 (2) (2002) 367–379.
[7] Y.C. Kweona, M.H. Kim, Experimental study on nucleate boiling enhancement and bubble dynamic behavior in saturated pool boiling

using a nonuniform dc electric field, Int. J. Multiphase Flow 26 (2000) 1351–1368.
[8] F.D. Moore, R.B. Mesler, The measurement of rapid surface temperature fluctuations during nucleate boiling of water, AIChE J. 7 (4) (1961) 620–624.
[9] C.M. Voustsinos, R.L. Judd, Laser interferometric investigation of the microlayer evaporation phenomenon, J. Heat Transfer 97 (1975) 88–92.
[10] Z.X. Guo, M.S. El-Genk, Liquid microlayer evaporation during nucleate boiling on the surface of a flat composite wall, Int. J. Heat Mass Transfer 37 (1994) 1641–1655.
[11] J.L. McGrew, F.L. Bamford, T.R. Rehm, Marangoni flow: an additional mechanism in boiling heat transfer, Science 153 (1966) 1106–1107.
[12] S. Petrovic, T. Robinson, R.L. Judd, Marangoni heat transfer in subcooled nucleate pool boiling, Int. J. Heat Mass Transfer 47 (2004) 5115–5128.
[13] H.K. Forster, N. Zuber, Dynamics of vapor bubbles and boiling heat transfer, Am. Inst. Chem. Eng. J. 1 (1955) 531–535.
[14] H.K. Forster, R. Greif, Heat transfer to a boiling liquid—mechanism and correlation, J. Heat Transfer 81 (1) (1959) 43–53.
[15] I.G. Shekriladze, On the role of the pumping effect of a vapor bubble growing at the wall during nucleate boiling, in: Voprosy konvektivnogo teploobmena I chistoty vodianogo para, Metsniereba Press, Tbilisi, 1970, pp. 90–97 (in Russian).
[16] I.G. Shekriladze, Sh.A. Mestvirishvili, J.G. Rusishvili, G.I. Zhoszholiani, V.G. Ratiani, Studies in the mechanism of boiling and of enhancement of evaporative cooling coefficients, Heat Transfer-Sov. Res. 12 (2) (1980) 91–95.
[17] X.F. Peng, Y.J. Huang, D.J. Lee, Transport phenomenon of a vapor bubble attached to a downward surface, Int. J. Therm. Sci. 40 (9) (2001) 797–803.
[18] H. Wang, X.F. Peng, B.X. Wang, D.J. Lee, Jet flow phenomena during nucleate boiling, Int. J. Heat Mass Transfer 45 (6) (2002) 1359–1363.
[19] H. Wang, X.F. Peng, W.K. Lin, C. Pan, B.X. Wang, Bubble-top jet flow on microwires, Int. J. Heat Mass Transfer 47 (2004) 2891–2900.
[20] R. Marek, J. Straub, The origin of thermocapillary convection in subcooled nucleate pool boiling, Int. J. Heat Mass Transfer 44 (3) (2001) 619–632.
[21] D.M. Christopher, B.X. Wang, X.F. Peng, Flow field around a condensing and evaporating vapor bubble in microgravity, in: Proc. Molecular and Microscale Heat Transfer in Material Processing and Other Applications, Part 2, 1996, pp. 162–170.
[22] H. Wang, X.F. Peng, D.M. Christopher, W.K. Lin, C. Pan, Investigation of bubble-top jet flow during subcooled boiling on wires, Int. J. Heat Fluid Flow 26 (2005) 485–494.
[23] J.A. Dean, Lange's Handbook of Chemistry, McGraw-Hill, New York, 1992.
[24] H.S. Lee, H. Merte Jr., Spherical vapour bubble growth in uniformly superheated liquids, Int. J. Heat Mass Transfer 39 (1996) 2427–2447.
[25] A.J. Robinson, R.L. Judd, The dynamics of spherical bubble growth, Int. J. Heat Mass Transfer 47 (2004) 5101–5113.
[26] R.R. Sharp, The nature of liquid film evaporation during nucleate boiling, NASA TND-1997, 1964.